Adhesive switching of membranes: Experiment and theory

Robijn Bruinsma,[1] Almuth Behrisch,[2] and Erich Sackmann[2,*]
[1]*Department of Physics, University of California, Los Angeles, California 90024*
[2]*Physik Department, E22 (Biophysical Laboratory), Technische Universität München, James Franck Straße, D-85747 Garching, Germany*
(Received 6 August 1999)

We report on a study of a model bioadhesion system: giant vesicles in contact with a supported lipid bilayer. Embedded in both membranes are very low concentrations of homophilic recognition molecules (contact site A receptors) competing with higher concentrations of repeller molecules: polyethylene glycol (PEG) lipids. These repellers mimic the inhibiting effect of the cell glycocalyx on adhesion. The effective adhesive interaction between the two membranes is probed by interferometric analysis of thermal fluctuations. We find *two competing states of adhesion*: initial weak adhesion is followed by slower aggregation of the adhesion molecules into small, tightly bound clusters that coexist with the regions of weak adhesion. We interpret our results in terms of a *double-well intermembrane potential*, and we present a theoretical analysis of the intermembrane interaction in the presence of mobile repeller molecules at a fixed chemical potential that shows that the interaction potential indeed should have just such a double-well shape. At a fixed repeller concentration we recover a conventional purely repulsive potential. We discuss the implications of our findings in terms of a general amplification mechanism of the action of sparse adhesion molecules by a nonspecific double-well potential. We also discuss the important role of the Helfrich undulation force for the proposed scenario.

PACS number(s): 87.16.Dg, 87.15.By

I. INTRODUCTION

Adhesion is a central problem in many areas of cell biology, as exemplified by the fact that more than 21 000 publications have appeared on this subject over the last six years, many of them concentrating on the molecular basis of cell-cell recognition and cell-tissue interaction [1]. Cell adhesion plays a key role in embryological development [2], immune response [3], and the pathology of tumors. Adhesive interactions also can be considered as one of the ''senses'' of a cell, which allows it to recognize nearby cells and to detect mechanical stresses.

By now, a large number of cell surface receptors and lipophilic ligands involved in the cell adhesion process have been identified, and their functionality and specificity have been characterized. There are two groups. ''Homophilic'' receptors are *self-recognizing*. For instance, the Ca^{2+}-dependent cadherin family of receptors [4] plays an important role during the early development of embryos. A second class of adhesion molecules is ''ligand-receptor'' pairs. A receptor binds to a particular target molecule, the ligand, whose molecular structure is stereo complementary to that of the receptor allowing molecular recognition: the ''lock-and-key'' model of Fischer [5]. Integrin receptors [6] recognize, for instance, specific peptide sequences of particular macromolecules of the extracellular matrix, such as fibronectin, collagen, and laminin. Once groups of integrins on the cell surface are connected to the extracellular matrix, linkages to the cytoskeleton are established that are associated with a cascade of cell signaling events [7]. This clustering of adhesion molecules (''focal adhesion sites'') is a common theme encountered in cell adhesion [8].

Cell surfaces are extremely complex, and relatively little is understood concerning the ''engineering design'' of cell adhesion, i.e., the key structural elements of cell membranes that allow them to operate simultaneously as efficient chemical sensors and efficient clamping devices. Typical surface concentrations of adhesion molecules are *very low* (usually of the order of 100 receptors per square micron), yet successful recognition by lock-and-key pairs can produce large-scale changes in cell shape, in combination with cell signaling [3]. Having low receptor concentrations certainly is a sensible cell design feature (because it avoids using up valuable space on the crowded cell surface, and because it reduces costly production of proteins) but how can so few molecules have such a large effect?

A classical model of cell adhesion was formulated by Bell, Dembo, and Bongrand [9] (called the BDB model below) to address this question. This model states that cell adhesion is governed by the competition between ''specific'' and ''generic'' interactions. The specific interaction is the above-mentioned lock-and-key recognition between adhesion molecules. The generic interaction is in part produced by the well-known classical forms of interaction between pure lipid membranes [10], the van der Waals attraction, the double-layer repulsion, the hydration repulsion, and the Helfrich entropic repulsion. Under physiological conditions, pure lipid bilayers adhere to each other with a binding energy W of the order of 0.1 mJ/m^2. We will refer to this either as ''primary'' or ''van der Waals'' adhesion. A second nonspecific form of interaction is provided by the headgroups of glycoproteins and by glycolipid molecules embedded in the cell surface [11]. These molecules form a ''repeller'' polymer brush, with a thickness in the range of 5–50 nm (depending on cell type), known as the *glycocalyx*. The BDB model assumes that this glycocalyx repulsion is strong enough to prevent van der Waals adhesion because nonspecific clustering of cells must be avoided. The role of receptors and ligands is to allow for specific recognition between cells. The size of the receptor-ligand pairs should at least be

*Author to whom correspondence should be addressed.

comparable to that of the glycocalyx to allow for rapid recognition kinetics.

The BDB model has provided us with a compelling physical framework to understand cellular adhesion, and one that has been largely confirmed over the years, but a number of serious questions remain to be answered. The model does not seem to account for *close* contact between two membranes. In the adhesive state envisioned in the BDB model, the two membranes are simply tethered by a sparse concentration of lock-and-key pairs but they are still separated by (roughly) the width of the glycocalyx. In many problems of cell adhesion (e.g., those involving cell fusion), *tight* contacts between the two membranes is required [12]. Also no mechanism is provided for the formation of focal adhesion sites. It might be assumed that specific mechanisms could reduce the intermembrane spacing and produce formation of adhesion-molecule clusters. Note, however, that the clustering of the adhesion molecules would have to ''switch on'' only *after* recognition or else the sparse receptors and ligands would cluster beforehand, in which case the lock-and-key recognition kinetics would become prohibitively slow.

In this paper we report on a combined quantitative and analytical study of membrane adhesion to investigate these questions: do adhesion molecules merely act as tethers or staples between two membranes or can they spontaneously produce focal adhesion sites, and what are the physical conditions under which tight adhesion can be achieved by adhesion molecules that are typically of the order of 10 nm? The ultimate goal would be to refine the BDB model so that it can provide us with design conditions that an artificial biomembrane has to obey in order for it to act as an efficient bio-adhesion system.

Because of the complexity of cell surfaces, for our study we have used a ''bioanalog'' model system: giant lipid dioleoyl-phosphatidylcholine (DOPC) bilayer vesicles with embedded adhesion molecules and embedded repeller molecules [see Fig. 1(b)]. Similar models were developed earlier for nonbiological adhesion molecules such as Biotin-Streptavidin ligand-receptor pairs [13] and anionic-cationic lipid pairs [14]. These studies indicated that low concentrations of adhesion molecules indeed have a tendency to aggregate spontaneously. In our present study, we recruited a biologically relevant adhesion molecule: the homophilic contact site A (csA) adhesion molecules [15] of *Dictyostelium discoideum* [see Fig. 1(a)]. This glycoprotein exhibits structural similarities to intracellular adhesion molecules (ICAM-1) [3], with a head group that contains three domains with structures similar to that of the IgG antibodies. It is attached to the membranes by a lipid anchor. CsA is essential for the development of *Dictyostelium* colonies from individual cell assemblies. Reconstituted csA molecules were used in an earlier micropipette study of vesicle adhesion [16] that reported that the csA molecules were freely mobile in the bilayer but that adhesion affected the csA distribution.

To model the glycocalyx, a significant concentration (5 mol %) of polyethylene glycol lipid (PEG-lipid, called ''repellers'') was also embedded in the vesicle surface. Figure 1(b) shows a schematic view of the two bilayers. The width of the model repeller coat (about 5 nm) was chosen to be comparable in size to that of the csA adhesion molecule (about 8 nm), as stipulated by the BDB theory. Homophilic

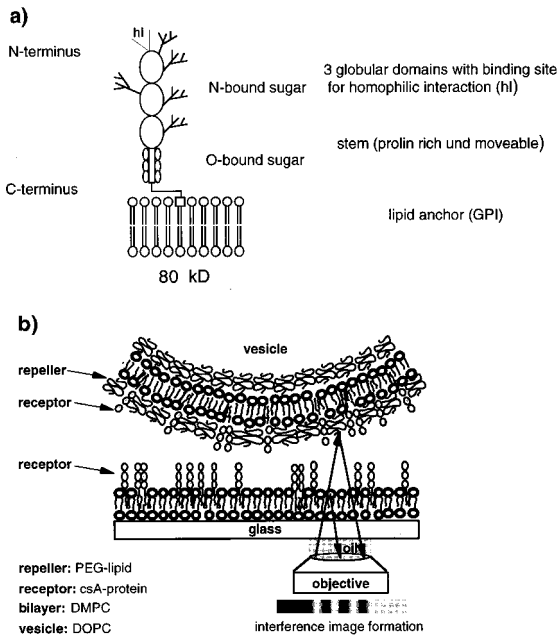

FIG. 1. A model system for bioadhesion. (a) Schematic view of contact site A (csA) receptors. The outer segment is composed of three domains to which N-linked oligosaccharides are coupled. The inner protein domain is coupled to the headgroup of the lipid anchor and is covered by O-linked sugars. The lipid anchor consists of a ceramide with a glycosyl-phosphatidyl inositol head group. (b) Adhesion between a test ''cell'' (a giant vesicle) and target ''tissue'' (supported membrane). Lock-and-key forces are simulated by interaction between homophilic cell adhesion molecules (contact site A proteins of *Dictyostelium discoideum*). An artificial glycocalyx is produced by reconstitution of lipopolymers in both membranes.

pairing of csA molecules should produce only a modest deformation of the repeller coat.

To monitor quantitatively the state of adhesion between the two membranes, we used the ''fluctuation analysis'' method [17]. In this microinterferometric technique, the adhesion disk is examined by reflection interference contrast microscopy (RICM). Analysis of the interference patterns allows for a detailed, quantitative, time-resolved determination of the position-dependent spacing profile between two membranes. These spacing profiles are found to exhibit thermal Brownian motion. The strength of these thermal fluctuations is a sensitive measure of the local adhesion strength. In particular, the fluctuation analysis provides us with the second derivative of the membrane-membrane interaction potential at the equilibrium spacing.

Theoretical analysis (see Sec. III) shows that if the membrane spacing is comparable to the width of the repeller coat or larger, then thermal fluctuations should be very clearly visible in the spacing profile. If, on the other hand, the two membranes are locally clamped together in regions of tight adhesive contacts, then the thermal fluctuations should be nearly completely quenched. The RICM method allows us in this manner to monitor the adhesion strength of different parts of the adhesion disk. In addition, it also provides us with other forms of quantitative information such as the adhesion-induced membrane tension γ as well as the lateral pressure Π of the adhesion disk. Finally, thermal fluctuations are not just important as a monitor of the state of adhesion:

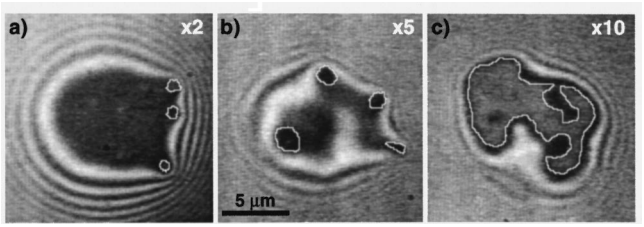

FIG. 2. RICM images of the adhesion disc. Tightly bound adhesion plaques appear dark (indicated by white contours). Weakly adhering regions exhibit a spotlike texture of thermally excited spacing fluctuations. (a), (b), and (c) show adhesion disks with increasing mole fractions X_p of adhesion molecules (see Table 1). (a) shows an average of 30 frames, and (b) and (c) show an average of 60 frames.

they also will play a direct and important role in the adhesion process itself as discussed in more detail in Sec. IV.

We can summarize the main results of our study as follows. The central experimental finding is that csA homophilic adhesion molecules show *multiple, competing states of adhesion*: early weak adhesion is followed by later strong adhesion. When the vesicle first comes into contact with the substrate, an adhesion disk forms exhibiting strong thermal fluctuations. These fluctuations are visible as time-dependent spotted patterns, with rms spacing fluctuations of the intermembrane distance in the 15–20-nm range (see Fig. 2, light gray-tone regions). With time, small sectors of strong adhesion appear (black-tone regions encircled by white lines in Fig. 2) showing little evidence of thermal fluctuations (rms spacing fluctuations below 10 nm). The total area fraction of these strong-adhesion plaques is proportional to the mole fraction of adhesion molecules and grows with time (see Fig. 3). Importantly, the formation of the tight adhesion spots is *not* an irreversible binding process: provided the domains are small (<0.5 μm), thermal fluctuations are strong enough to cause tight-adhesion domains to disappear. Our results thus indicate that tight-adhesion spots can form spontaneously and reversibly, and that they compete with a state of weak adhesion. In other words, focal adhesion sites can form spontaneously. The observed patterns of weak and strong adhesion regions show clear similarities with those observed in earlier experiments on the simpler adhesion systems, indicating that a generic mechanism is at work.

Can we understand the observed multistage adhesion scenario in terms of an intermembrane potential energy? For pure lipid bilayers under conditions of high salinity, this potential energy is well known to be the sum of a long-range van der Waals attraction and a short-range repulsion. Figure 4(a) shows a typical calculated potential energy per unit area $V(h)$ [the parameters are approximately appropriate for dimyristoyl-phosphatidylcholine (DMPC)]. The adhesion free energy per unit area W is the depth of the potential well so it is equal to $-V(h^*)$, with h^* the position of the potential minimum (in the range of 2–3 nm). The results of experiments with the surface force apparatus (also called the force box below) on lipid bilayers are consistent with this potential [18]. In Fig. 4(b) we show the effect of including a *fixed* surface concentration of polymer molecules with a radius of gyration of 5 nm. The surface concentration was taken to be close to the overlap concentration. This new potential energy is very weakly attractive for large h (beyond 10 nm) but strongly repulsive for smaller h. Force-box experiments [19] on lipid bilayers with embedded PEG-lipid repellers confirm this description.

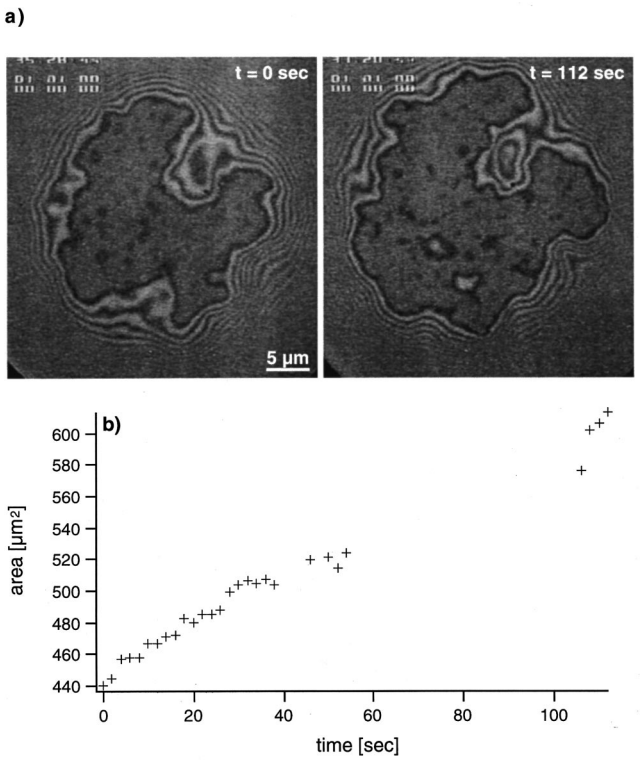

FIG. 3. Growth with time of strong adhesion plaques. (a) Adhesion disk immediately following settling of the vesicle on the substrate (left frame) and after 120 sec (right frame). (b) Time evolution of the area of strong-adhesion patches (measured in μm^2). Note that the growth process appears to consist of a fast initial stage and a slower later stage.

It seems difficult to reconcile our findings with a repulsive intermembrane potential energy resembling Fig. 4(b). Formation of dimer csA adhesion pairs should locally restrict the intermembrane spacing to at most the size of two csA molecules (about 16 nm). This is comparable to or larger than the size of the polymer brush, so thermal fluctuations should still be quite visible. The absence of thermal fluctuations indicates that the tight adhesion plaques have an intermembrane spacing of just a few nm (although RICM does not permit direct measurement of mean spacing profile in spacing range).

It is a central claim of this paper that the intermembrane potential energy appropriate for membrane adhesion experiments has in fact a second minimum for small spacings. To justify this claim, we note that for states of *microadhesion*—such as the observed tight-adhesion plaques—the repeller concentration must be locally altered by the state of adhesion, as recently stressed by Bongrand [20]. The adhesion molecules do remain in chemical equilibrium with the nonadhering parts of the membrane so the intermembrane potential $V(h)$ must be computed at a *fixed chemical potential*, not at a fixed repeller concentration. The result of such a calculation is shown in Fig. 5 (see Sec. III). We obtain a surprising, nonmonotonic ''double-well'' potential with a sharp minimum for small h and a broad minimum for large h. The

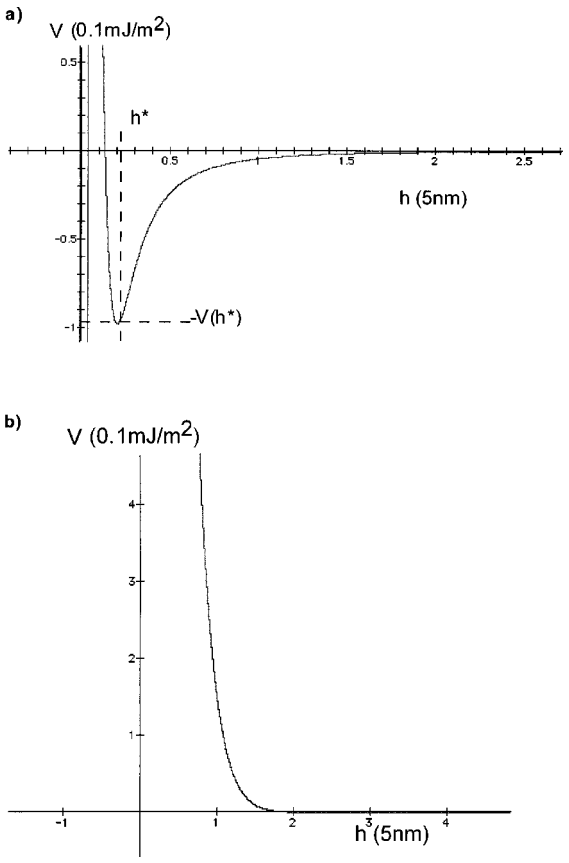

FIG. 4. Intermembrane potential energy per unit area as a function of the intermembrane spacing h. (a) Van der Waals attraction plus short-range repulsion. The Hamaker constant and membrane thickness are those of DMPC. The strength of the short-range repulsion was adjusted to fit the measured adhesion energy of 0.1 mJ/m^2. The equilibrium spacing is less than that of DMPC. (b) Same as (a), but now including the effect of a fixed concentration of repeller polymers attached to one membrane. The polymers have a radius of gyration R_g of 5 nm, and the surface concentration σ was fixed at $\sigma R_g^2 = 2.5$.

primary minimum $h(I)$ is close to that of the ''bare'' van der Waals potential of Fig. 4(a), and the shape of the potential energy per unit area indeed resembles the bare potential energy of Fig. 4(a). *There is, however, a net upward shift in energy equal to the two-dimensional osmotic pressure* $k_BT\sigma_0$ *of the repeller coat*. The adhesion energy per unit area of the primary minimum thus equals $V(h(I)) = k_BT\sigma_0 - W$.

To interpret the experimental observations in terms of this potential, we identify the weak adhesion state with the secondary minimum and the strong adhesion state with the primary minimum. In Sec. III we will show that the primary minimum indeed should exhibit only very weak thermal fluctuations, consistent with our observations on the tight-adhesion sites. The secondary minimum is predicted to be in the range of 10 nm, and it should show very strong thermal fluctuations, consistent with observations on the weak-adhesion state. The thermal fluctuations of the secondary minimum in fact appear to be sufficiently strong to cause ''thermal unbinding'' [21]. If generic adhesion is to be avoided, as required by the BDB model, then thermal unbinding of the secondary minimum would be a reasonable design condition.

If we now vary the concentration of repeller molecules, and follow the evolution of the two minima of the potential, then, for low repeller osmotic pressure, the primary minimum is the absolute minimum of the potential. When the repeller concentration is increased, a first-order phase transition takes place near the point where $V(h(I))$ changes sign, i.e., the point where the repeller osmotic pressure $k_BT\sigma_0$ is equal to the ''bare'' adhesion energy W (similar phase transitions produced by long-range interactions are familiar from the Cahn theory of wetting [22]). W is about 0.1 mJ/m^2 for DMPC, and, for repeller molecules with radii of gyration in the 5 nm range, and concentrations close to the overlap concentration, the two-dimensional (2D) osmotic pressure also is about 0.1 mJ/m^2. At the critical point $W = k_BT\sigma_0$, the absolute minimum shifts from $V(h(I))$ to $V(h(II))$. A consistent interpretation of our experiments is now possible by assuming that our model system happens to be close to this first-order phase transition point. Let H be the local spacing a bonded pair of adhesion molecules imposes on the intermembrane spacing h (more precisely, h must be less than, or equal to, H at the site of a bonded pair). Let a collection of adhesion molecules locally restrict the membrane spacing to be less than H. As shown in Fig. 5, *if the potential energy per unit area* $V(H)$ *exceeds* $V(h(I))$, *then tight*-adhesion plaques form spontaneously by locally forcing a transition from the secondary to the primary minimum. In terms of the theory of first-order phase transitions, the adhesion molecules can be said to act like *pretransitional nucleation* sites. The resulting ''plaque'' would contract spontaneously, once tight adhesion was established, because the plaque is still under a compressive 2D pressure equal to $V(h(I))$ applied by the part of the membranes that is not in the adhesion plaque. This pressure would concentrate the adhesion molecules to form a dense, compacted region until the 2D compression is in balance either with the 2D osmotic pressure of the concentrated pairs of bound adhesion molecules or with the 2D pressure generated by short-range steric repulsive forces between the adhesion molecules.

An objection to this scenario is that we have not provided a mechanism showing how such clusters of csA adhesion molecules should form (csA molecules embedded in reconstituted membranes in fact aggregate spontaneously but only over times scales larger than 3 h). As noted, similar decomposition processes were observed in earlier model adhesion studies indicating that a nonspecific mechanism is at work. Bruinsma, Goulian, and Pincus [23] (BGP) showed that a significant, nonspecific attraction between bonded adhesion molecules can appear if bonding of adhesion molecules imposes a free energy cost due either to enthalpic or entropic repulsion between the two membranes. An elegant laser-tweezer experiment by Bar-Ziv *et al.* [24] analyzed in Ref. [25] illustrated this point by showing that the pinching together of two membranes produces a strong unbinding in the surrounding area. Two adhesive links thus would ''prefer'' to be closely associated. In Sec. IV, we will apply the BGP results to derive a Flory mean-field phase diagram for adhesion molecules (shown in Fig. 8 below). We will show that the adhesion disk is indeed expected to decompose spontaneously even at very low concentrations of bonded pairs.

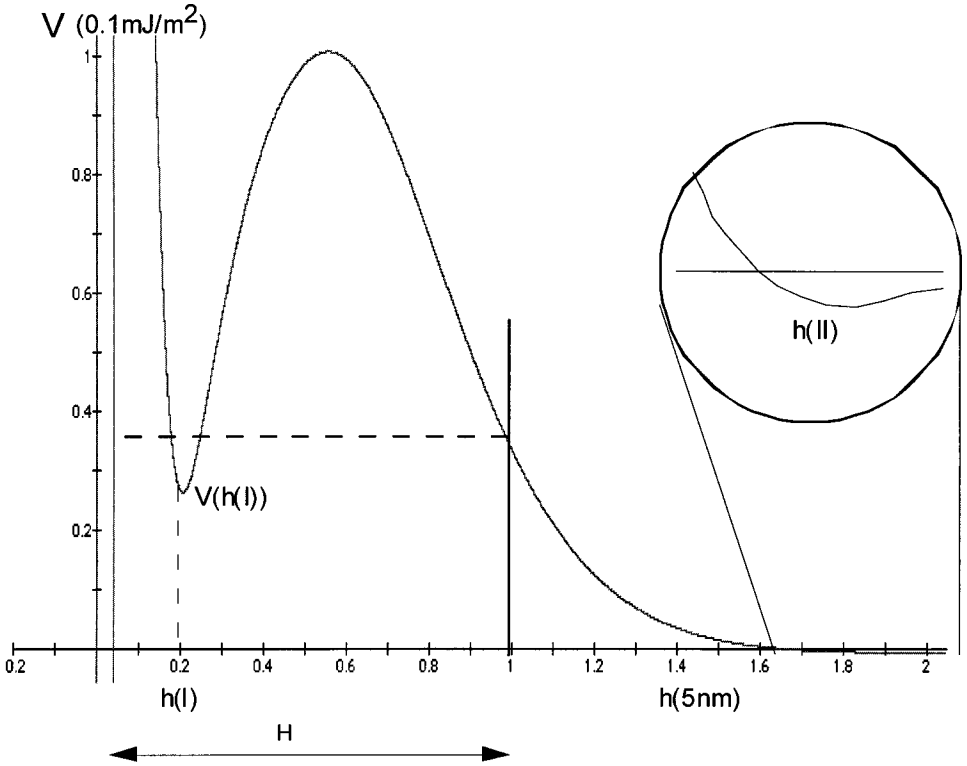

FIG. 5. Intermembrane potential energy per unit area at fixed chemical potential. The parameters are the same as those of Fig. 4(b), but the potential energy was computed at fixed chemical potential. The chemical potential was chosen such that $\sigma R_g^2 = 2.5$ for large h. The position of the primary minimum is indicated by $h(I)$, and that of the shallow secondary minimum by $h(II)$.

The adhesion molecule concentration of the experiments discussed in Sec. II is in fact close to the phase-boundary line for decomposition shown in Fig. 8.

We will finish this summary by examining the consequences of our experimental and theoretical results for the BDB model and the design of bio-adhesion membranes. In the BDB model, bioadhesion molecules act like ''staples,'' attaching two membranes together through their binding energy. Our results indicate that it is likely that a more sophisticated scenario is at work: *adhesion molecules act like adhesion regulators* by controlling the access to the primary or van der Waals minimum of the double-minimum generic potential energy. The double-well potential thus *amplifies* the effect of the adhesion molecules. This is an appropriate arrangement for the design of biomembranes, since low concentrations of regulatory adhesion molecules can produce large effects. Two-stage adhesion (with rapid initial adhesion followed by slower, but stronger, final adhesion) has in fact also been reported for the adhesion of real cells [20]. Our results appear to indicate that the csA/PEG-lipid system is an excellent model system for the study of bioadhesion.

Although the experimental results can be consistently interpreted within the framework of the theory, specific quantitative tests remain necessary. The theory predicts, for instance, that the size of the tight-adhesion spots should increase significantly as the repeller concentration σ_0 aproaches the threshold W/k_BT, and this prediction has not yet been checked. The theory also predicts that reducing the adhesion molecule concentration by a factor of 10 or so below the value used in the current experiment should lead to the disappearance of the tight adhesion spots. Preliminary experiments indeed find that at lower csA concentrations no adhesion plaque formation is observed. The vesicles settle transiently on the substrate but unbind constantly.

II. EXPERIMENT

A. Sample preparation

The giant vesicle and the supported membrane of the model system discussed in the Introduction were composed of DOPC and DMPC, respectively. Lock-and-key forces were established by reconstitution of cell surface contact site A (csA) homophilic protein receptors from cells of *Dictyostelium discoideum*. Figure 1(a) shows a model of the receptor. The outer section is composed of three Ig-like domains which are connected by flexible hinges [see Fig. 1(a)]. The inner domain is rich in proline and threonine and exhibits O-linked oligosugars that act as protection against proteases. An important advantage of csA molecules is that they have lipid anchors composed of a *g*lycosyl *p*hosphatidyl *i*nositol (GP) anchor that can be easily reconstituted. In addition, they diffuse rapidly in membranes. In order to model the glycocalyx, a solution of about 5 mol % of lipopolymers composed of phosphatidylethanolamine with polyethyleneoxide (PEO) headgroups (''PEG lipids'') where reconstituted in the vesicle membranes. These lipopolymers also greatly assist the formation of single walled vesicles. The PEO section of the molecule was composed of 45 monomers. The Flory radius of a polymer of that size is about 5 nm. At a 5-mol % surface concentration, the PEG lipids should provide a uniform polymer brush covering the DOPC surface with a width in excess of 5 nm (because of the lateral compression of the PEG lipids).

TABLE I. First row: Concentration of csA protein in giant vesicles in mole fractions. Second row: Relative area fraction of strongly adhering adhesion patches A_a/A_{10}, where A_a and A_{10} are areas of tight adhesion patches and weakly adhering regions, respectively. Third row: Average spreading pressures S of strong adhesion plaques.

	$\times 1$	$\times 2$	$\times 5$	$\times 10$	$\times 20$
Protein mole fraction x_P	4×10^{-6}	8×10^{-6}	2×10^{-5}	4×10^{-5}	8×10^{-5}
Relative area of tight contacts	0.03	0.04	0.50	0.9	1.6
Average spreading pressure S of strong adhesion plaques (J/m^2).	5×10^{-7}	10^{-7}	-	10^{-7}	5×10^{-7}

The purification of the receptors, and the preparation of the supported membranes and of the vesicles, as well as the characterization of their essential structural and physical properties, were described in a preceding paper [26], and will be only briefly summarized. The supported membranes were deposited by the monolayer transfer technique. First, an inner monolayer of DMPC was deposited at a lateral pressure of 26.5 mN/m and 25 °C. Before deposition of the outer monolayer (by the Langmuir-Schäfer technique) the solubilized csA protein was injected into the subphase at an initial monolayer lateral pressure of 24 mN/m. Reconstitution of the monolayer was monitored by observation of the increase in lateral pressure. The adhesion experiments were performed within 3 h following preparation to avoid slow csA aggregation. Transfer took place after saturation of the pressure increase, typically after 1–2 h. The total amount of csA injected into the sub-phase was 50 pMo. The *absolute* concentration of reconstituted csA could not be determined [28], however. Assuming that *all* the proteins injected were reconstituted would lead to a total area concentration c_s (subscript S stands for supported membrane) of about $c_s \approx 10^{-2}$ proteins/nm^2, corresponding to a maximum lipid-to-protein molar ratio of 100:1 (or a protein molar fraction $x_P \approx 10^{-2}$). Inspection of the distribution of receptors in the supported membrane by microfluorescence showed that the proteins appeared to be randomly distributed, at least on μm scales, although some small clusters of higher concentration were observed at submicrometer resolution by electron microscopy [27]. Reconstitution of csA in the bilayers of the giant vesicles was achieved by incubation of a suspension of vesicles and solubilized receptors. The concentrations were much lower in this case: about $10^{-5}-10^{-6}$ mol fractions (see Table I for receptor concentrations). The reason for our interest in membrane adhesion at very low adhesion molecule concentrations was discussed earlier.

The fluidity of the supported membrane was characterized by first measuring the lateral diffusion coefficient of a fluorescence lipid analog using the fluorescence-recovery-after-photobleaching (FRAP) technique. We obtained a diffusion constant $D_{\rm lat}$ of about 3×10^{-8} cm^2/sec which is about a factor of 2–3 smaller than a typical lipid diffusion constant in free bilayers. The diffusion of csA was then estimated by observation of the slow formation of clusters of csA in a monolayer containing fluorescent lipid analog. Small nonfluorescent clusters appeared after about 5 h with an average spacing of about 100 μm. We thus estimate the diffusion coefficient D of csA in the support layer to be about 10^{-9} cm^2/sec.

Finally, to allow the vesicles to settle on the substrate, a weak gravitational force was generated through a density contrast between the inner and outer phases of the vesicle. The outer phase consisted of 10-mM Hepes buffer and the inner of 10-mM raffinose corresponding to a density difference of $\Delta\rho \sim 3$ kg/m^3.

B. Measurement methods

Observations were performed by RICM. These images are formed by interference of light waves reflected from the substrate surface and the adherent cell surface. The adherent and nonadherent sections of the vesicle can be clearly distinguished, since the latter leads to a series of fringes that follow the locus of lines of equal height above the surface. Due to the finite coherence of the illuminating light, the fringes can only be observed up to a height of about 1 μm (if the slope of the tangent to the vesicle surface is less than 30°). Measurement of the interference fringes allows a reconstruction of the intermembrane spacing profile in a direction perpendicular to the rim of the adhesion disc. This method allows a determination of the position and structure of the rim of the adhesion disc (defining the contact line of the partially wetting vesicle) as well as the structure of the pattern of strong and weak adhesion patches.

Analysis of the height profile provides us with the effective contact angle ϑ' and with the ''extrapolation length'' λ (the distance between the edge of the adhesion disk and the linearly extrapolated vesicle profile far from the edge). These two quantities provide access to important physical parameters characterizing the adhesion process. Vesicle adhesion necessarily produces a tension γ in the vesicle surface, even if the vesicle was initially flaccid. An application of the theory of elastic shells to membrane adhesion [26,28] shows that the extrapolation length is given by $\lambda = \sqrt{\kappa/\gamma}$, with κ the Helfrich bending energy of the membrane. The bending energy can be obtained, by the flicker-analysis method, from the nonadhering vesicle [17,29], so measurement of the extrapolation length provides us with the value of the adhesion-induced tension. Next, the quantity $S = \gamma(1-\cos\theta)$ plays the role of a *spreading pressure* of the adhesion disk. For a one-component lipid bilayer with no adhesion molecules, this pressure is simply equal to the adhesion free energy per unit area W (i.e., the Young-Dupré Law). For multicomponent membranes with embedded adhesion molecules, the interpretation of S is more delicate (and contentious), in particular if strong binding between adhesion molecules produces nonequilibrium effects. There are however two simple limiting cases

(i) *Fixed chemical equilibrium* If an adhesion disk is in full chemical equilibrium with the remainder of a (large)

vesicle or support, then S can be equated with the Gibbs free energy of adhesion per unit area G. In an earlier study of vesicle adhesion [14] (by charged lipids) we found that G is in fact much smaller than W when adhesion-induced phase-separation takes place producing paired adhesion molecules inside the adhesion disk. The Young-Dupré Law is in general invalid for bioadhesion problems.

(ii) *Fixed number of adhesion molecules* If the adhesion disk contains a *fixed number* of tightly bound (but mobile) pairs of adhesion molecules—i.e., if the ligand receptor binding energy is very high—then S can be interpreted as the sum of the nonspecific adhesion free energy plus the 2D pressure of the many-body system of paired adhesion molecules [30]. This 2D pressure is again quite low compared to the van der Waals adhesion energy.

As noted, for the present experiment, smaller csA adhesion plaques were observed to unbind by thermal fluctuations but not the larger ones. This indicates that our sample is actually in neither of the two simplifying limiting cases so S should be interpreted with caution.

We now turn to observations of the adhesion process. Figures 2 and 3 show that the adhesion disk decomposes into two states: areas of constant dark tone which will be called ''adhesion plaques'' (encircled by white lines), and regions of weak adhesion that are characterized by a leopard-like texture. This characteristic pattern is a consequence of the pronounced temperature induced Brownian fluctuations of the membrane. We measured the total area of the strong and weak states of adhesion (A_s and A_w, respectively) as a function of the receptor concentration of the vesicle. The area ratios were measured for five different csA molar fractions. The relative area fractions A_s/A_w of the strong adhesion plaques are given in Table I. By plotting the total area fraction $\varepsilon=(A_s/A_s+A_w)$ of tight adhesion as a function of the protein area fraction x_P, one finds that ε increases roughly *linearly* with the receptor concentration in the vesicles, indicating that the adhesion molecules control the size of the adhesion plaques. This rules out the possibility that the primary minimum of the potential energy of Fig. 5 has a negative value, since in that case the adhesion molecules would act as nucleation sites of a first-order phase transition and the adhesion plaque area would not be proportional to the csA concentration.

Small adhesion plaques form spontaneously at random sites immediately after gravity-induced settling of the vesicles on the substrate and then grow rapidly. An example of the growth process is shown in Fig. 3. There appear to be two stages: an initial fast-adhesion process with a rise time of about 10 sec followed by a slower stage which saturates after about 50–100 sec. If we assume that the growth of the adhesion plaques is a diffusion controlled process, then the average time τ required for the receptors to diffuse over a distance of the order of the vesicle radius R is about $\tau \approx R^2/D$. For a typical vesicle radius of $R\approx 10\,\mu$m the fast growth time of 10 sec would correspond to a diffusion coefficient of the csA molecules in the support layer of about $D\approx 10^{-9}\,\mathrm{cm}^2/\mathrm{sec}$, in good agreement with the value discussed earlier for monolayers. This indicates that the growth of adhesion plaques is a diffusion-limited process.

As mentioned, the RICM method permits us to measure fluctuations of the intermembrane spacing profile. In Fig. 6 we show examples of spacing profiles for both weak and strong adhesion regions. As noted earlier, the vesicle membrane performs strong thermal fluctuations in regions of weak adhesion, while the tight-adhesion plaques show only weak evidence for thermal fluctuations. We performed a statistical analysis of the time sequence of the local intensity fluctuations of the RICM micrographs. From the intensity fluctuations, we obtained the mean square amplitude $\sqrt{\langle u^2\rangle}$ of the intermembrane spacing fluctuations [13]. Figure 6 shows plots of $\sqrt{\langle u^2\rangle}$ along two sections of vesicles with csA molar fractions of $x_P\approx 4\times 10^{-6}$, $x_P\approx 4\times 10^{-5}$, and $x_P\approx 8\times 10^{-5}$ in arbitrary units. Note the two coexisting states of adhesion. By application of the theory of RICM image formation [3], we find that the weakly adhering regions have fluctuation amplitudes $\sqrt{\langle u^2\rangle}$ of about 20 nm, while $\sqrt{\langle u^2\rangle}$ is smaller than 10 nm for the strongly adhering regions (close to the limit of resolution of the method). For comparison, in Fig. 6(b) we show the case of a strongly adhering vesicle with a homogeneous adhesion disk where $\sqrt{\langle u^2\rangle}<10\,\mathrm{nm}$. The method permits measurement of the fluctuation profile, but it is not sufficiently precise for measurement of mean spacings in the 10-nm range.

The spreading pressure S of the adhesion plaques was measured, by the method discussed above, and was found to be less than a microjoule per square meter (see Table I), which is small compared with the spreading pressure W due to the van der Waals interaction for pure lipid bilayers (about $0.1\ \mathrm{mJ/m}^2$).

III. INTERMEMBRANE POTENTIAL ENERGY

A. Bare intermembrane potential energy

The interaction potential per unit area $V(h)$ of single-component DMPC lipid bilayers, spaced a distance h, with no repeller molecules, has been extensively studied theoretically and tested both through force-box measurements [18] and by thermal-diffuse x-ray diffraction. For DMPC, $V(h)$ exhibits a single minimum at a bilayer spacing h^* of about 2.4 nm with a binding energy W of about $0.1\ \mathrm{mJ/m}^2$. At $h=h^*$, the van der Waals attraction is in balance with short-range steric repulsion (DMPC is neutral so there is no double-layer repulsion). To find an explicit expression for $V(h)$, assume two neutral parallel bilayer membranes in aqueous environment, each with a thickness δ (about 3.5 nm for DMPC). The intermembrane potential energy per unit area $V(h)$ is then the sum of a short-range steric repulsion V_s and the van der Waals potential V_{vdW}:

$$V_{\mathrm{bare}}(h)=V_s(h)+V_{\mathrm{vdW}}(h), \tag{3.1}$$

The short-range term can be represented empirically as [31]

$$V_s=V_0e^{-h/\lambda}, \tag{3.2}$$

with V_0 usually of the order of k_BT per molecule and with a ''screening length'' λ of the order of 2 Å. The van der Waals interaction between two layers is given by

$$V_{\mathrm{vdW}}(h)=-\frac{H_A}{12\pi}\left(\frac{1}{(h+2\delta)^2}+\frac{1}{h^2}-\frac{2}{(h+\delta)^2}\right), \tag{3.3}$$

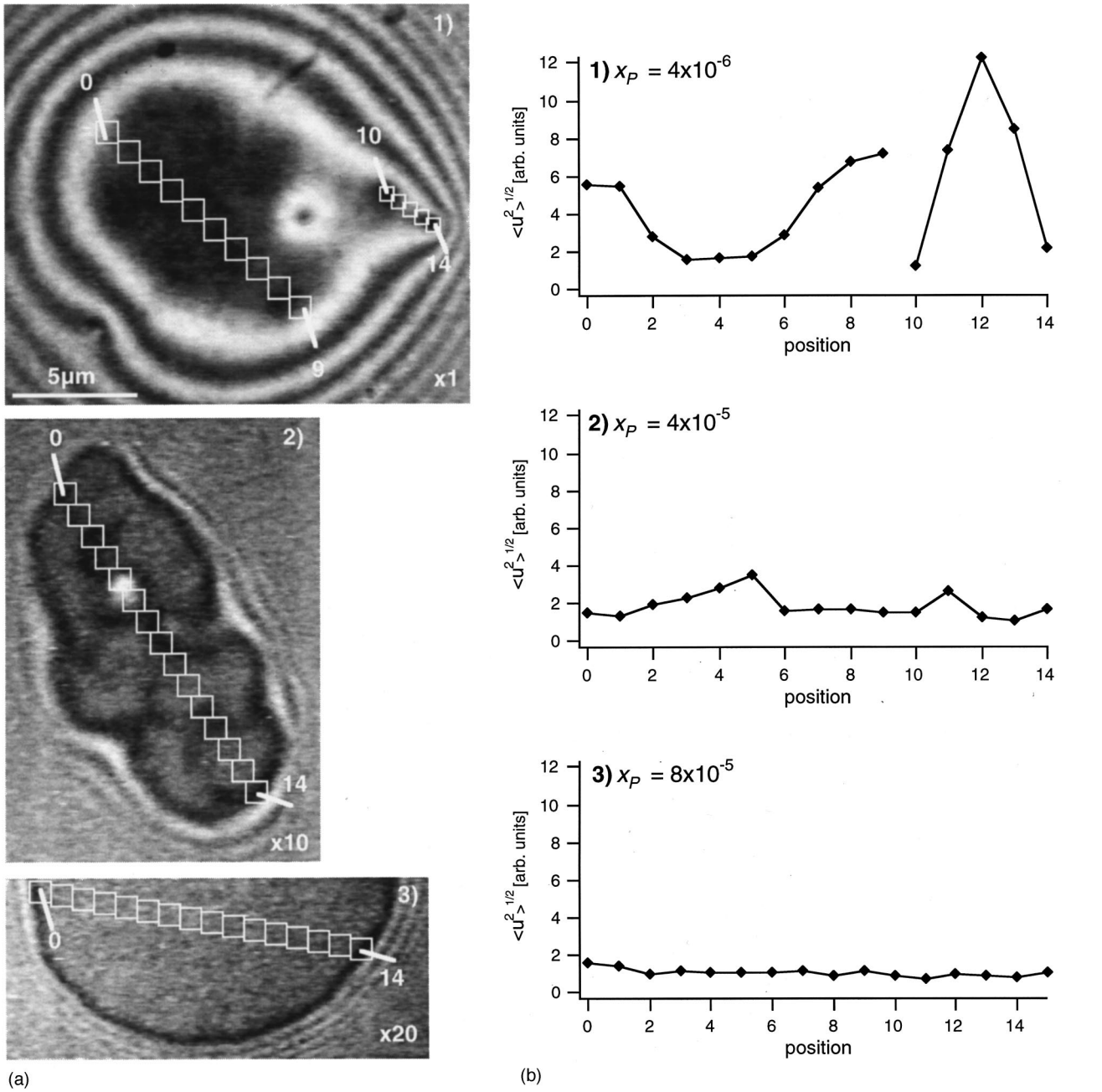

FIG. 6. Measurement of the rms amplitude of thermal flickering along sections across the adhesion disc. (a) RICM micrographs of vesicles containing csA molar fractions of (1) 4×10^{-6}, (2) 4×10^{-5}, and (3) 8×10^{-5}, respectively. They exhibit coexisting stongly adhering and weakly adhering regions. (b) Plot of rms amplitudes along sections marked by squares on RICM micrographs for (1), (2), and (3). The numbers along the horizontal axis of the graphs correspond to the number of the square in the RICM images. Note that squares 10–14 in (1) show a section between two pinning centers.

with H_A the Hamaker constant (about 7×10^{-21} J for DMPC). We will refer to Eq. (3.1) as the ''bare potential.'' This bare potential must have a minimum of the order of 0.1 mJ/m^2 for DMPC. In Fig. 4(a) we show $V(h)$, where we adjusted V_0 by hand to fit the measured binding energy. Note that the predicted equilibrium spacing is somewhat too small. In addition to Eq. (3.1), there is also a weak long-range gravitational attraction between the vesicle and the surface due to the density contrast between vesicle and solution.

B. Repeller potential energy: Fixed concentration ensemble

Let σ_0 be the surface concentration of repellers. Each repeller is treated as a neutral polymer with a radius of gyration R_g. There is no closed form for the entropic free energy cost of a polymeric layer attached to one plate and confined by a second plate. However, for concentrations below or near the overlap concentration (i.e., $\sigma_0 R_g^2<1$), this cost can be approximated by

$$V_{\mathrm{rep}}(h)\cong\frac{\pi^2}{6}k_BT\sigma_0\left(\frac{R_g}{h}\right)^2 e^{-1.5(h/R_g)^2} \tag{3.4}$$

This is an approximate interpolation formula, which reduces for small h to the well known Dolan-Edwards expression of

a polymer confined between two plates [32]. In the other limit, for spacings h larger than the radius of gyration, the steric energy cost should be of the order of k_BT per repeller times the Gaussian probability that the chain is extended over a distance h from the attachment site.

Note that for small h both the entropic confinement cost and the van der Waals attraction depend on h as $1/h^2$. Steric repulsion dominates over attraction provided the following condition is obeyed:

$$2\pi^3 \frac{k_BT}{H_A}\sigma_0 R_g^2 > 1. \tag{3.5}$$

Near the overlap concentration, the left hand side of Eq. (3.5) is of the order of 30 (using parameters appropriate for DMPC). We conclude that even for repeller concentrations considerably below the overlap concentration, the entropic free energy cost of compressing the polymer still exceeds the van der Waals attraction. In Fig. 4(b), we show the sum of $V_{\rm bare}(h)$ plus $V_{\rm rep}(h)$. The radius of gyration of the polymers was set at 5 nm and the repeller concentration σ_0 was set equal to the experimental value ($\sigma_0 R_g^2 = 2.5$). The resulting interaction is indeed repulsive for small h. Note that there is a very shallow minimum—denoted by $h(II)$—for h near 10 nm. The reason is that for large h the repeller potential energy decays as a Gaussian but the van der Waals attraction decays as a power law, so for large h the attraction dominates. Experimentally, the interaction between lipid bilayers with embedded PEG lipids was measured by Kuhl *et al.* [19] with the force-box method, and the interaction was found to be uniformly repulsive, even at quite low PEG-lipid concentrations. This is consistent with the above discussion, and with previous estimates of the strength of the repeller potential.

Note that we implicitly assume that the repeller concentration remains fixed. When two (nearly) flat macroscopic membrane sectors are brought into contact, as is, for instance, the case in a force-box experiment, then the potential of Fig. 4(b) indeed is appropriate because the mean repeller concentration could only change very slowly (by long-range transport to the edge).

C. Repeller potential energy: Fixed chemical potential ensemble

As mentioned in Sec. I, for problems involving microadhesion—as for the tight-adhesion plaques seen experimentally—we must compute the Gibbs free energy of adhesion at a fixed chemical potential $\mu = k_BT \ln \sigma_0 \Omega$, with Ω the area per repeller head group and σ_0 the repeller surface concentration far from the adhesive region (thus $\sigma_0 \Omega$ is dimensionless). To compute this potential, let $\sigma(h)$ be the local repeller concentration inside an adhesive contact. The repeller chemical potential is the sum of the usual translational entropy term plus the cost of compression of the polymer tails as described by Eq. (3.4). The Gibbs equilibrium condition demands that this local chemical potential equals the fixed chemical potential μ:

$$\mu = k_BT \ln \Omega\sigma(h) + \frac{\pi^2}{6} k_BT \left(\frac{R_g}{h}\right)^2 e^{-1.5(h/R_g)^2} \tag{3.6}$$

It follows from Eq. (3.6) that the repeller concentration $\sigma(h)$ depends on the spacing h as

$$\sigma(h)/\sigma_0 = \exp\left[-\frac{\pi^2}{6} k_BT \left(\frac{R_g}{h}\right)^2 e^{-1.5(h/R_g)^2}\right]^{1/2}. \tag{3.7}$$

According to Eq. (3.7), if the spacing h is small compared to the radius R_g of gyration, then the repeller concentration inside the adhesion plaque is strongly reduced. The Gibbs free energy per unit area $G(\sigma)$ of the repeller coat is then

$$G(\sigma) = k_BT\sigma(\ln(\Omega\sigma) - 1) + \frac{\pi^2}{6} k_BT\sigma \left(\frac{R_g}{h}\right)^2 e^{-1.5(h/R_g)^2}. \tag{3.8}$$

The effective intermembrane thermodynamic potential energy is $V_{\rm rep}(h) = G(\sigma(h)) - G(\sigma_0)$. Using Eqs. (3.7) and (3.8), we find

$$V_{\rm rep}(h) = k_BT\sigma_0 \left\{1 - \exp\left[-\frac{\pi^2}{6}\left(\frac{R_g}{h}\right)^2 e^{-1.5(h/R_g)^2}\right]\right\}, \tag{3.9}$$

The limiting behavior of this potential is given by

$$V_{\rm rep}(h) = \begin{cases} k_BT\sigma_0 \dfrac{\pi^2}{6}\left(\dfrac{R_g}{h}\right) e^{-1.5(h/R_g)^2}, & h \gg R_g \\ k_BT\sigma_0, & h \ll R_g. \end{cases} \tag{3.10}$$

For large h, we thus recover the repeller potential energy at fixed concentration [see Eq. (3.4)]. For small h, the repulsive potential saturates at a value equal to the asymptotic two-dimensional osmotic pressure $\Pi = k_BT\sigma_0$ of the repeller coat.

In Fig. 7 we show the total potential energy of interaction $V(h)$, the sum of the bare potential energy [Eqs. (3.1) and (3.9)] for different values of $\sigma_0 R_g^2$. $V(h)$ has two minima. The primary minimum is located at the same spacing $h(I)$ as the minimum of the bare potential. The secondary minimum is at the same position as the shallow minimum of Eq. (3.1). For repeller concentrations exceeding approximately $\sigma_0 R_g^2 \cong 0.6$, the secondary minimum is the absolute free energy minimum while for repeller concentrations below $\sigma_0 R_g^2 \cong 0.6$ the primary minimum is the lowest free energy.

This means that the system undergoes a first-order phase transition as a function of the (dimensionless) parameter $\sigma_0 R_g^2$ from a state with the equilibrium intermembrane spacing set by the thickness R_g of the repeller coat to a state with a spacing set by the bare potential. The location of the first-order transition is determined by the condition that the osmotic pressure Π of the repeller coat just equals the bare binding energy W:

$$k_BT\sigma_0 = W. \tag{3.11}$$

For $W = 0.1\ \mathrm{mJ/m^2}$, this critical surface concentration corresponds to one repeller molecule per 4000 A^2, which is a typical repeller concentration used in the present experiments.

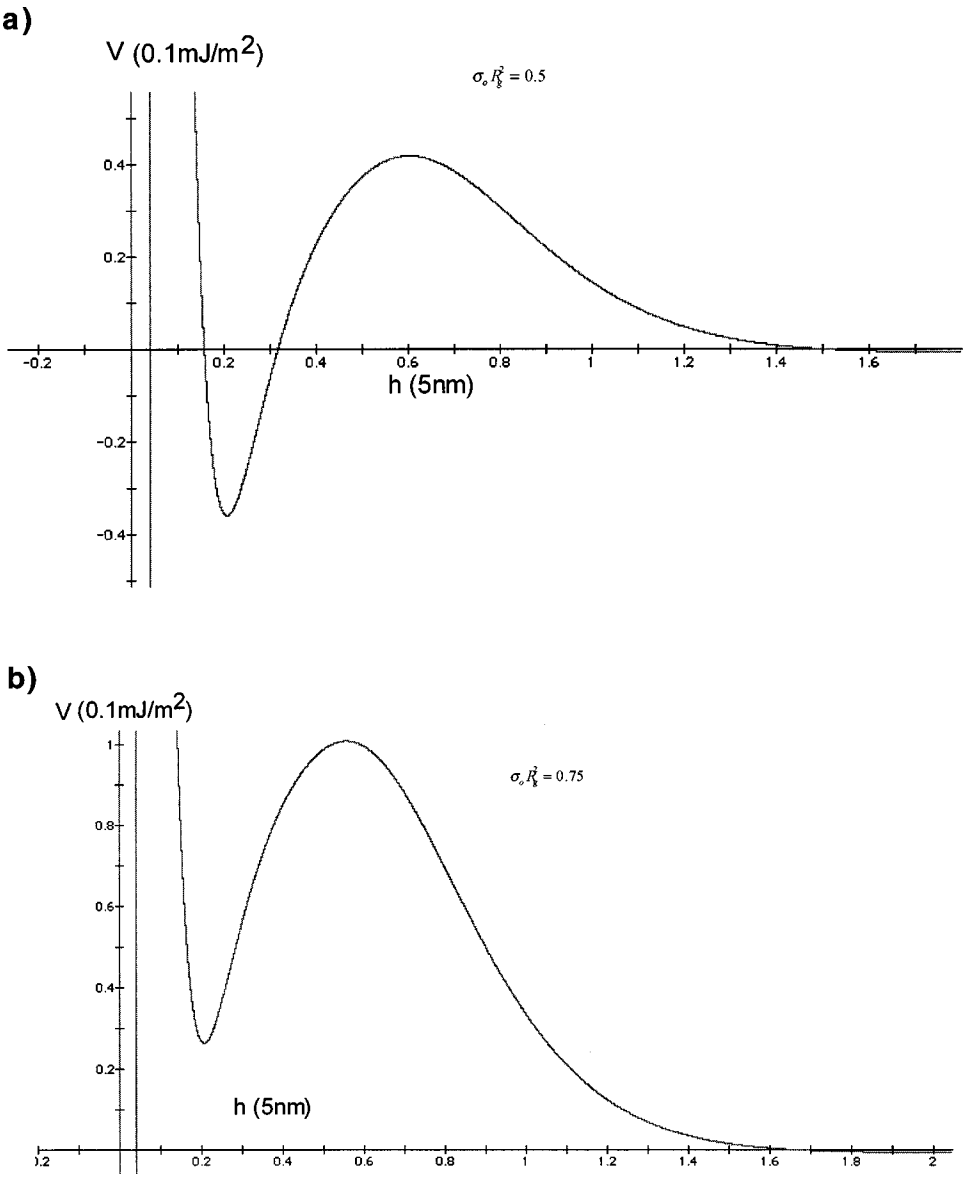

FIG. 7. Total potential energy for two different values of $\sigma_0 G_g^2$. $V(h)$ has a primary minimum and a secondary minimum. Note that for (a) $\sigma_0 G_g^2 < 0.6$ the primary minimum is the absolute free energy minimum, while for (b) $\sigma_0 G_g^2 > 0.6$ the secondary minimum is lower than the primary minimum.

D. Thermal fluctuations and thermal unbinding

In this section we briefly discuss the effect of thermal fluctuations on the two different states of adhesion. Expand the (full) potential energy per unit area $V(h)$ in a Taylor series around either minimum h^*:

$$V(h) \cong V_0 + \frac{V''}{2}(h-h^*)^2. \tag{3.12}$$

In Eq. (3.12), the depth of the primary minimum of $V(h)$ is of the order of $10^{-5}\,\mathrm{J/m^2}$ with a curvature V'' of the order of $10^{14}\,\mathrm{J/m^4}$. The depth of the secondary minimum V_0 is considerably smaller, of the order of $10^{-6}\,\mathrm{J/m^2}$, while V'' is of the order of $10^{12}\,\mathrm{J/m^4}$ for the secondary minimum.

To characterize the thermal fluctuations, we use the harmonic elastic energy functional of a soft membrane in a harmonic potential [33]

$$H = \frac{1}{2}\int d^2r\{\kappa(\nabla^2 u)^2 + \gamma(\nabla u)^2 + V'' u^2\}, \tag{3.13}$$

where $u = h - h^*$ is the deviation of the membrane spacing from the minimum of the potential, κ is the Helfrich bending modulus (about $15 k_B T$ for DMPC), while γ is the adhesion-induced membrane tension. There are two characteristic length-scales in H, the extrapolation length λ we encountered earlier,

$$\lambda = \left(\frac{\kappa}{\gamma}\right)^{1/2}, \tag{3.14}$$

and the correlation length

$$\xi = \left(\frac{\kappa}{V''}\right)^{1/4}. \tag{3.15}$$

The correlation length is the distance it takes for a perturbation in h to relax back to h^*.

Recall that the extrapolation length can be measured from the spacing profile at the edge of the adhesion disk [26]. We found it to be about 1 μm (see Table I). From the known value of $\kappa \approx 10^{-19}$ J of DMPC, Eq. (3.14) gives an adhesion tension $\gamma \approx 10^{-7}$ N/m. The correlation length ξ of the secondary minimum is about 20 nm, while the correlation length of the primary minimum is about 10 nm. From the fact that the correlation length is very short compared to the extrapolation length, we can deduce the fact that the tension term in Eq. (3.13) plays no role at the submicron length scales relevant to the present case.

Using standard methods, it is straightforward to compute the mean square $\langle u^2 \rangle$ of the spacing fluctuations from Eq. (3.13):

$$\langle u^2 \rangle = \frac{1}{2} \frac{k_B T}{\kappa} \xi^2, \tag{3.16}$$

Using our estimated values for the correlation lengths of the two minima, and a value $15 k_B T$ for the bending energy, we find an estimated rms $\sqrt{\langle u^2 \rangle}$ of the height fluctuations of about 4 nm for the secondary minimum and one of about 1 nm for the primary minimum (this difference in rms values between the two minima is the theoretical basis for using a fluctuation analysis to monitor the state of adhesion).

Equation (3.16) implicitly assumes that thermal fluctuations do not affect the state of adhesion. As mentioned in Sec. I, thermal fluctuations can, however, also produce thermal *unbinding* [21], with much larger values of $\sqrt{\langle u^2 \rangle}$. To test for this possibility, we compute the lowest order correction to the adhesion free energy due to thermal fluctuations

$$V_{\text{eff}} \cong V_0 + \frac{V''}{2} \langle u^2 \rangle \cong V_0 + \frac{k_B T}{4\kappa} V'' \xi^2. \tag{3.17}$$

The secondary minimum no longer represents a state of true adhesion if V_{eff} is positive. Using our earlier estimates for the correlation length we find $(V''/2)\langle u^2 \rangle \approx 7 \times 10^{-6}$ J/m^2 for the secondary minimum. This exceeds significantly the binding energy of the secondary minimum. The state of weak adhesion is thus expected to exhibit very strong thermal fluctuations (the membranes do not completely unbind due to the gravitational force on the vesicle). On the other hand, the thermal fluctuations correction to the primary minimum binding energy is small. The contrast of $\sqrt{\langle u^2 \rangle}$ between primary and secondary states thus should be quite large indeed, and should be visible within the precision of the RICM method (about 10 nm).

IV. SELF-ASSEMBLY OF FOCAL ADHESION SPOTS

In this section we examine under which conditions even very low concentrations of adhesion molecules can aggregate spontaneously to form focal adhesion sites in the absence of specific bonding between the adhesion molecules. Paired adhesion molecules locally deform the membrane. The resulting membrane-mediated interactions between adhesion molecules can depend either on the bending stiffness of the membrane [23] (the BGP theory), or on the adhesion-induced membrane tension [34]. As discussed in above, bending energy effects dominate for length scales less than the extrapolation length. This is in the micron range for the present experiment, so we will focus on interaction mediated by bending stiffness.

We will describe a pair of bonded csA adhesion molecules as a local constraint on the membrane spacing h: if a pair of adhesion molecules is located at a position R (measured along the support membrane), then

$$h(R) \leqslant H. \tag{4.1}$$

Adhesion molecules like the csA receptors are assumed to be structurally flexible, so they does not affect the local intermembrane spacing provided h is less than H. The free energy gain per bound pair of adhesion molecules will be denoted by ΔE. This binding free energy must be obtained either by a measurement of the equilibrium constant for the binding reaction between adhesion molecules in solution, or by molecular modeling. Typically, ΔE is in the range of $(10-20) k_B T$ for biologically relevant adhesion molecules [for instance, $\Delta E \sim 15 k_B T$ for the integrin/fibronectin pair or $\Delta E \sim (15-25) k_B T$ for antigen-antibody pairs under standard conditions]. We shall see that membrane-bound csA molecules probably have a binding energy in the same range. We will briefly review the BGP results and then apply them to construct a Flory mean-field phase diagram.

A. Membrane-mediated interaction between adhesion molecules

1. Single pair of adhesion molecules

Assume there is just a single pair of bonded adhesion molecules. The glycocalyx is locally compressed by the pair. The deformation free energy cost U is computed by minimizing the elastic energy functional [Eq. (3.13)] under the constraint [Eq. (4.1)] with the result [23]

$$U = \begin{cases} 8 V''(H - h^*)^2 \xi^2, & H < h^* \\ 0, & H > h^*. \end{cases} \tag{4.2}$$

Note that U is roughly the energy cost required to squeeze the glycocalyx by an amount $h^* - H$ over a disk of a radius of the correlation length ξ. Assuming $h^* = h(\text{II}) = 10$ nm and $\xi = 20$ nm, we find U to be $0.6 k_B T$ and $2.4 k_B T$ for H equal to 8 and 6 nm, respectively. We conclude that energy cost required for the deformation of the glycocalyx is modest in the present case.

2. Two pairs of adhesion molecules

Now assume two pairs of bonded molecules, separated by a distance R. The free energy of the two pairs, $F_2(R)$, can be shown to be

$$F_2(R) = -2\Delta E + \frac{2U}{1 + \dfrac{\text{kei}(R/\xi)}{\text{kei}(0)}}, \tag{4.3}$$

with kei(x) the Thompson function. From the asymptotic expansion of the Thompson function, it follows that

$$F_2(R) \approx \begin{cases} 2F_1 - U\left(\dfrac{\xi}{2R}\right)^{1/2} \sin(R/\sqrt{2}\xi) e^{-R/\sqrt{2}\xi}, & R \gg \xi \\ 2F_1 - U, & R \ll \xi, \end{cases} \tag{4.4}$$

where $F_1 = -\Delta E + U$. Note that that the correlation length ξ is a measure of the range of a membrane-mediated pair interaction between adhesion molecules, and that U also sets the energy scale for the binding between pairs of adhesion molecules.

3. Entropic interactions

It is well known that thermal fluctuations generate entropic repulsion between neighboring membranes: the Helfrich entropic repulsion. In BGP theory, this leads to an additional entropic energy cost for the binding of adhesion molecules given by

$$\Delta F^1_{\text{entr}} \cong 2\pi\sqrt{2\alpha} k_B T \ln \frac{L}{\xi}, \tag{4.5}$$

with α a numerical factor of the order 0.1, and L the radius of the adhesion disk. For an adhesion disk with a radius of 10 μm, and for ξ equal to 20 nm, this entropic energy cost is considerable, of the order of $15 k_B T$. The entropic free energy of two adhesion molecules separated by a distance R depends logarithmically on their spacing:

$$\Delta F^2_{\text{entr}}(R) \cong \Delta F^1_{\text{entr}} + 2\pi\sqrt{2\alpha} k_B T \ln \frac{R}{\xi}. \tag{4.6}$$

Entropic attraction is not pairwise additive. Using variational methods, it can be shown that the entropic energy cost per adhesion site of a (hexagonal) array of N paired adhesion molecules, with an area of πR^2 per molecule, must be less than

$$\Delta F^{\text{array}}_{\text{entr}}(R) \cong N T k_B T \ln \frac{R}{\xi}, \tag{4.7}$$

Like Eq. (4.6), this depends logarithmically on the spacing R, but the numerical prefactor $\Gamma = 2\sqrt{\pi\alpha} \cong 1.12$ is considerably smaller than that of Eq. (4.6).

B. Flory mean-field theory

To obtain the phase diagram of adhesion molecules interacting via the membrane-mediated interactions we just detailed, we will use the Flory mean-field theory. We will treat the substrate as an infinite reservoir of mobile adhesion molecules with the adhesion molecule chemical potential μ fixed at

$$\mu = k_B T \ln a_0 \delta, \tag{4.8}$$

with δ the surface number density of adhesion molecules embedded in the support membrane, and a_0 the area of a csA molecule (making $a_0 \cdot \delta$ a dimensionless quantity). Under the conditions described in Sec. II, the adhesion molecule mole fraction $a_0\delta$ is of the order 10^{-5}–10^{-6} and the csA chemical potential is of the order $\mu \approx (11$–$14) k_B T$. The vesicle will be treated as a finite reservoir containing a fixed number N of embedded adhesion molecules, so, if A_ν is the vesicle area, then the surface concentration is $\delta = N/A_\nu$. We will treat the adhesion disk as a reactive two-component solution of fixed area. The adhesion molecules embedded in the top (+) and bottom (−) membranes play the roles of the two reacting species. The reactive solution is in chemical equilibrium both with the vesicle and the support membrane. We will use the standard description of chemical reactions, and including the nonideality of the solution by the pair potential discussed in Sec. IV A.

We want to compute the mole fraction X of pairs of bonded adhesion molecules inside the adhesion disk. This mole fraction has a maximum value $X_{\max}$ when all N adhesion molecules of the vesicle are collected in the adhesion disk. If the area of the adhesion disk is A_{ad}, then $X_{\max} = a_0\delta(A_\nu/A_{ad})$, which is of the order of 10^{-6} for the experiments described in Sec. II. For a given mole fraction X, the mean spacing R between pairs of adhesion molecules is related to X by $R = (a_0 X)^{-1/2}$.

In Flory mean-field theory, the Gibbs free energy $G(X)$ per unit area of our nondeal two-dimensional solution would be given by

$$G(X) \cong G_{\text{ideal}}(X) - \frac{\Gamma}{2} k_B T (X/a_0) \ln\left(X \frac{\xi^2}{a_0}\right) - \frac{1}{2} z (U/a_0) X^2, \tag{4.9}$$

where z is the maximum number of nearest neighbors. The first term of $G(X)$ is the Gibbs free energy of a reactive binary mixture in dilute solution, while the last two terms describe correlation effects. Before discussing the correlation effects, we will first briefly review the prediction of ideal-solution theory.

The Gibbs free energy for the case of an ideal, reactive mixture is

$$\begin{aligned} G_{\text{ideal}}(X)/a_0 = {} & k_B T\{X \ln X + (1-X)\ln(1-X)\} \\ & - 2\mu X - (\Delta E - U) X + (X_{\max} - X) k_B T \\ & \times \ln\left(1 - \frac{X}{X_{\max}}\right) + X k_B T. \end{aligned} \tag{4.10}$$

It is the sum of the mixing entropy, the chemical potential gain per unit area of removing two unpaired adhesion molecules from a reservoir with a chemical potential μ per molecule, and of the free energy gain $\Delta E - U$ of the chemical reaction. Finally, the last two terms of Eq. (4.10) describe the additional entropic free energy cost for adhesion that is encountered because the adhesion disk reduces the concentration of adhesion molecules of the finite-sized vesicle. If we minimize $G_{\text{ideal}}(X)$ with respect to X for the case of an infinite vesicle, i.e., without the last two terms, we find

$$X_{\text{ideal}} = \frac{1}{1 + e^{(\Delta E - U - 2|\mu|)/k_B T}}. \tag{4.11}$$

In the strong-bonding limit $\Delta E \gg 2|\mu|$, the mole fraction of sites with bonded molecules inside the adhesion disk would be close to one in this regime. If, however, we include the finite-size term of Eq. (4.10), then we find that, for $\Delta E \gg 2|\mu|$, the mole fraction X instead saturates at the maxi-

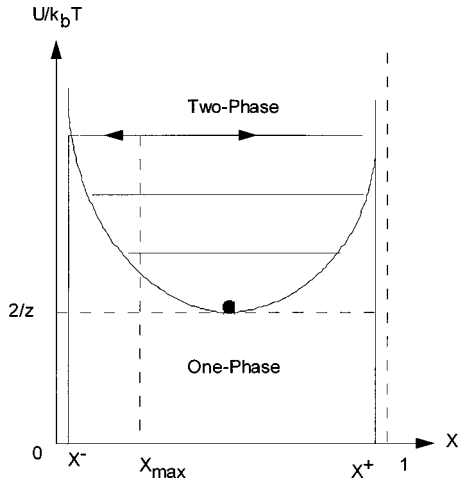

FIG. 8. Phase diagram of state of adhesion where U/k_BT is the reduced Flory parameter and X is the molar fraction of ligand pairs.

mum value $X_{\max}$. In the weak bonding limit $\Delta E \ll 2|\mu|$, the mole fraction is close to zero. In ideal-solution theory, definite ''recognition'' between membranes with embedded adhesion molecules thus requires the binding energy to exceed $\Delta E = 2|\mu|$. For the present case this means that ΔE should exceed $(20-30)k_BT$ since $\mu \sim (10-15)k_BT$.

Finally, we include the correlation terms of Eq. (4.9). The second term of Eq. (4.9) represents the entropic interaction [Eq. (4.7)], and the third term the short-range pair potential [Eq. (4.2)]. We will assume that the maximum number of near neighbors in a densely packed patch of adhesion molecules is $z=6$. If we now minimize $G(X)$ with respect to X than we find that, for the numerical estimates for U found in Sec. IV A the correlation terms have little effect on the optimal value for X and for $\Delta E \gg 2|\mu|$, the optimal mole fraction X is still approximately equal to $X_{\max}$.

Assume that $\Delta E \gg 2|\mu|$, so adhesion between the two membranes has been established and the average mole fraction of bonded molecules inside the disk is fixed at $X_{\max}$. To discuss whether or not phase separation can take place, it is convenient to first go to an ensemble with fixed total particle number. Instead of the Gibbs free energy, the appropriate variational principle is then the Helmholtz free energy $F(X)$. After a Legendre transformation, we find, for $F(X)$,

$$F(X)a_0 \cong k_BT\{(1-\Gamma/2)X\ln X + (1-X)\ln(1-X)\} - \tfrac{1}{2}zU(X-1/2)^2. \tag{4.12}$$

$F(X)$ is very similar to the standard Flory free energy of a (nonreactive) two-phase binary mixture, with U playing the role of the Flory parameter. The phase diagram can be computed by standard methods [35], with the result shown in Fig. 8. The binodal phase boundary shown in Fig. 8 separates homogeneous solutions (small U) and phase-separated solutions (large U). The phase boundary line exhibits a maximum at a critical, or consolute, point. The value of U at the critical point is obtained from the conditions $\partial^3 F/\partial^3 X = \partial^2 F/\partial X^2 = 0$. For $\Gamma = 2\sqrt{\pi\alpha} \cong 1.12$, this gives $zU/k_BT \cong 2.75$. Corresponding to this, we thus expect two different forms of adhesion: (a) *Homogeneous regime* $zU/k_BT < 2.75$, where The adhesion disk is a dilute, homogeneous solution of paired adhesion molecules; and (b) *two-phase regime*: $zU/k_BT > 2.75$, where the disk spontaneously decomposes into dilute and dense regions provided the initial mole fraction $X = X_{\max}$ is within the interval X^+ to X^- indicated in Fig. 8. The phase-separated dilute and dense regions have surface concentrations of X^+ and X^-, respectively. For larger U, the bounds of the decomposition regime are given by

$$X^- \cong e^{(zU/k_BT)+\Gamma/2-\Gamma}, \qquad X^+ \cong 1. \tag{4.13}$$

The theory of this section thus allows for the spontaneous formation of tight focal adhesion sites (with X^+ close to one) for very low concentrations of adhesion molecules, provided two conditions are satisfied: (i) zU/k_BT exceeds 2.75, and (ii) the saturated adhesion molecule mole fraction $X_{\max}$ exceeds X^- as given by Eq. (4.13). Are these conditions reasonable for the experiments discussed in Sec. I? We saw earlier that U is of the order of a few k_BT, so the first condition is reasonable for $z=6$. Next, if we assume that the adhesion area is about one-tenth of the total vesicle area, then we find that the experimental value of $X_{\max}$ is in fact very close to X^-. Formation of adhesive patches is thus possible for very low concentrations of adhesion molecules and modest values of the deformation energy scale U. Note that thermal fluctuations substantially assist the formation of aggregates, through the factor Γ in Eq. (4.13). The accuracy of the theory is not such that we can be sure whether or not the second condition is actually satisfied. However, the theory does predict that if we would lower the csA concentration in the experiment by any significant amount, say a factor of 10, then no tight-adhesion spots should appear. Preliminary data show that this expectation is indeed verified. In fact, if we significantly lower the concentration of adhesion molecules then no adhesion at all is observed. Phase separation appears to be a necessary condition for proper adhesion.

V. SUMMARY AND CONCLUSION

The present extension of the classical BDB model of cell adhesion shows that the adhesion of mixed membranes containing small amounts of lock-and-key pairs and moderate concentrations of repeller molecules (mimicking the glycocalyx of cells) is controlled by lateral phase separation and receptor clustering. The intermembrane repulsion can be augmented by undulation forces. This is the consequence of the double-well intermembrane interaction potential generated by the competition between strong specific attraction between lock-and-key pairs and the generic repulsion between repeller molecules of opposing membranes together with the lateral osmotic pressure provided by the reservoir of repeller molecules. A further driving force for receptor clustering is lateral attraction between receptors. As a possible nonspecific coupling mechanism we postulated attraction between tightly bound lock-and-key pairs through a local deformation of the membrane at the transition between sites of tight-adhesion (pinning centers) and decoupled membrane regions. The double minimum potential can amplify the effect of a few sites of tight adhesion (acting as nucleation sites), and drive the ''first order'' transition into a state of

stronger adhesion by growth of the initial pinning centers into adhesion patches (similar to the nucleation and growth process during phase separation in alloys or polymer blends).

The question arises whether our postulated mechanism plays a role in cell adhesion which is often controlled by a small number of receptors (e.g., of the integrin family). There is substantial evidence that nonspecific mechanisms play a central role during cell adhesion. Thus evidence has been provided that adhesion of cytotoxic *T*-lymphocytes to their target cells such as white blood cells; e.g., lymphocytes may be controlled by diffusion-limited clustering of receptors and is more efficient when the receptors are mobile then when they are immobilized by coupling to the cytoskeletor [3]. In the experiments of Ref. [3] the lock and key pairs consisted of the GPI, anchored receptor (LFA-3, of a similar structure to that of csA) which was reconstituted into supported bilayers and a receptor (called CD2) in the *T*-lymphocyte membrane. The latter receptor is anchored to the cytoskeleton. An interesting postulate of these studies is that the initial process of cell adhesion does not necessarily require cell signalling. Lateral mobility of a receptor is also a basic requirement for the present model. A basic requirement for the validity of our model is that the receptor binding energy is of the order of $10k_BT$. This condition is often fulfilled for cell receptors (cf. Sec. I).

A key role in our cell adhesion model is played by the glycocalyx and a basic requirement is that the head groups of the repeller molecules extend similarly far into the extracellular space as the receptor head groups. Now many cell surface receptors exhibit rather large head groups. Thus headgroups of receptors of the *N*-CAM family are composed of up to five lg-like domains, and can protrude by 20 mm, while those of integrins can extend by 15 nm [36]. They thus extend considerably farther than typical head groups of glycolipids and even glycoproteins. However, the polymer coat of cells (such as lymphocytes) is much thicker (typically several 100 nm) due to the binding of giant protein filaments from the extracellular matrix (EM). Examples are fibronectins, proteoglycans and laminin coupled with one end to cell receptors. The role of repellers can also be played by oligosaccharides and polysaccharides of the EM such as hyaluronic acid (HA). Adsorbed monolayers of HA exhibit thicknesses of 50–90 nm depending on the ionic strength [37]. Nonspecifically adsorbed macromolecules in equilibrium with the bulk aqueous phase are expected to act similarly to membrane-anchored repeller molecules. The major difference is that their osmotic pressure can be regulated through the bulk concentration. Many adhesion competent cells (such as mesemchyme cells) can produce hyaluronic acid [2], and the enzymatic machinery is located in the plasma membrane which opens the possibility of interactive regulation of the generic repulsion forces. The huge hyaluronic acid molecules (hydrodynamic radius $\sim$500 nm) can indeed mimick the role of undulation forces, and lead to a local unbinding of the weakly adhering regions of the adhesion disc.

With the notable exception of erythrocytes, normal cells do not exhibit pronounced flickering since the lipid-orotein bilayer is coupled to the actin cortex. However, evidence of the flickering of normal mammalian cells (with amplitudes of $\sim$100 nm) have been provided in Ref. [38]. Moreover, recent studies of adhesion of endothelial cells in one of the authors laboratory (Erich Sackmann) showed that freshly adhering cells exhibit pronounced flickering with flicker rms amplitudes of 10 nm.

A further intriguing prediction of our adhesion model is that the free energy of adhesion can be controlled drastically through the chemical potential of the receptors in the nonadherent moiety of the cell surface. We showed that the spreading pressure can be reduced by several orders of magnitude through the two-dimensional osmotic pressure difference between the adherent and free regions of the membrane. Cells can thus control adhesion strength through internalization or enhanced genetic expression of cell surface receptors.

[1] For reviews see M. L. Turner, Biol. Rev. Cambridge Philos. Soc. **67**, 359 (1992); A. G. Lee, *Biomembranes* (JAI Press, Greenwich, CT, 1993), Vol. 3; P. Bongrand, Rep. Prog. Phys. **62**, 921 (1999).

[2] P. B. Toole, in *Proteoglycans and Hyaluronan in Morphogenesis and Differentiation in Cell Biology of the Extracellular Matrix*, edited by E. D. Hay (Plenum, New York, 1991), p. 305.

[3] P.-Y. Chan, M. B. Lawrence, M. L. Dustin, L. M. Ferguson, D. E. Golan, and T. A. Springer, J. Cell Biol. **115**, 245 (1991); M. L. Dustin, M. L. Ferguson, P.-Y. Chan, T. A. Springer, and D. E. Golan, *ibid.* **132**, 465 (1996).

[4] B. Gumbiner, Trends Biochem. Sci. **13**, 75 (1988).

[5] J. Wyman, and S. J. Gill, *Binding and Linkage. Functional Chemistry of Biological Macromolecules* (University Books, Los Angeles, 1990).

[6] R. O. Hynes, Cell **69**, 11 (1992).

[7] A. Howe, A. E. Aplin, S. K. Alahari, and R. L. Juliano, Curr. Opin. Cell Biol. **10**, 220 (1998).

[8] For reviews, see K. Burridge, K. Fath, T. Kelly, G. Nuckolls, and C. Turner, Annu. Rev. Cell Biol. **4**, 487 (1988); R. O. Hynes, Cell **48**, 549 (1987).

[9] G. I. Bell, M. Dembo, and P. Bongrand, Biophys. J. **45**, 1051 (1984).

[10] For a review, see J. N. Israelachvili, *Intermolecular and Surface Forces*, 2nd ed. (Academic, London, 1992).

[11] For a review, see C. Foa, M. Soler, A.-M. Benoliel, and P. Bongrand, J. Mater. Sci. **7**, 141 (1996).

[12] See, for instance, C. L. Adams and W. J. Nelson, Curr. Opin. Cell Biol. **10**, 572 (1998).

[13] A. Albersdörfer, T. Feder, and E. Sackmann, Biophys. J. **73**, 245 (1997).

[14] J. Nardi, R. Bruinsma, and E. Sackmann, Phys. Rev. E **58**, 6340 (1998).

[15] For reviews see C. Siu, BioEssays **12**, 357 (1999); J. Faix, G. Gerisch, and A. A. Noegel, J. Cell. Sci. **102**, 203 (1994).

[16] C. W. Maier, A. Behrisch, A. Kloboucek, and R. Merkel, in *Material Science of the Cell*, edited by B. Mulder, V. Vogel, and C. Schmidt (Materials Research Society, Boston, 1999).

[17] J. Rädler, T. J. Feder, H. H. Strey, and E. Sackmann, Phys. Rev. E **51**, 4526 (1995).

[18] J. Marra and J. Israelachvili, Biochemistry **24**, 4608 (1985).
[19] T. Kuhl, D. Leckband, D. Lasic, and J. Israelachvili, Biophys. J. **66**, 1479 (1994).
[20] P. Bongrand, Rep. Prog. Phys. **62**, 921 (1999).
[21] R. Lipowsky and S. Leibler, Phys. Rev. Lett. **56**, 2541 (1986).
[22] P. G. deGennes, Rev. Mod. Phys. **57**, 827 (1985).
[23] R. Bruinsma, M. Goulian, and P. Pincus, Biophys. J. **67**, 746 (1994).
[24] R. Bar-Ziv, R. Menes, E. Moses, and S. A. Safran, Phys. Rev. Lett. **5**, 3356 (1995).
[25] R. Menes, S. A. Safran, and D. Kessler, Europhys. Lett. **40**, 225 (1997).
[26] A. Kloboucek, A. Behrisch, J. Faix, and E. Sackmann, Biophys. J. **77**, 2311 (1999).
[27] A. Behrisch, Ph.D. thesis, TU-Munchen, 1998.
[28] R. Bruinsma, in *Physics of Biomaterials Fluctuations, Self Assembly, and Evolution*, Vol. 61 of *NATO Advanced Study Institute, Series 322: Applied Sciences*, edited by T. Riste and D. Sherrington (Dortrecht, Boston, 1996), p. 322.
[29] E. Sackmann, in *Handbook of Biological Physics*, edited by R. Lipowsky, and E. Sackmann (Elsevier/North-Holland, Amsterdam, 1995), Chap. 5, p. 213.
[30] See, for instance, D. Noppi-Simson and D. Needham, Biophys. J. **70**, 1391 (1996).
[31] A. Parsegian, N. Fuller, and R. P. Rand, Proc. Natl. Acad. Sci. USA **76**, 2750 (1979).
[32] P.-G. deGennes, *Scaling Concepts in Polymer Physics* (Cornell University Press, Ithaca, NY, 1979).
[33] U. Seifert and R. Lipowsky, Phys. Rev. A **42**, 4768 (1990).
[34] D. M. Zuckerman and R. Bruinsma, Phys. Rev. Lett. **74**, 3900 (1995); R. Lipowsky, *ibid.* **77**, 1652 (1996); D. M. Zuckerman and R. F. Bruinsma, Phys. Rev. E **57**, 964 (1998).
[35] See, for instance, *Scaling Concepts in Polymer Physics* (Ref. [32]), Chap. IV.
[36] J. J. Calvete, Tromb. Haemost. **72**, 1 (1994).
[37] A. Albersdörfer and E. Sackmann, Eur. Phys. J. B **10**, 663 (1999).
[38] L. Mittelman, S. Levin, and R. Korenstein, FEBS Lett. **293**, 207 (1991).